Crystallographic analysis of Polypyrimidine Tract-Binding Protein-Raver1 interactions Involved in Regulation of Alternative Splicing

Amar Joshi[1], Miguel B. Coelho[2], Olga Kotik-Kogan[1], Peter J. Simpson[3], Stephen J. Matthews[3], Christopher W.J. Smith[2] and Stephen Curry[1]

[1]Division of Cell and Molecular Biology
[3]Division of Molecular Biosciences,
Imperial College, Exhibition Road, London SW7 2AZ, UK.
[2]Department of Biochemistry, University of Cambridge, Tennis Court Road, CB2 1QW, UK.
*Correspondence: s.curry@imperial.ac.uk
DOI 10.1016/j.str.2011.09.020
http://www.cell.com/structure/abstract/S0969-2126(11)00333-9

SUMMARY

The polypyrimidine tract binding protein (PTB) is an important regulator of alternative splicing. PTB-regulated splicing of α-tropomyosin is enhanced by Raver1, a protein with four PTB-Raver1 Interacting motifs (PRIs) that bind to the helical face of the second RNA recognition motif (RRM2) in PTB. We present the crystal structures of RRM2 in complex with PRI3 and PRI4 from Raver1, which — along with structure-based mutagenesis — reveal the molecular basis of their differential binding. High-affinity binding by Raver1 PRI3 involves shape-matched apolar contacts complemented by specific hydrogen bonds, a new variant of an established mode of peptide-RRM interaction. Our results refine the sequence of the PRI motif and place important structural constraints on functional models of PTB-Raver1 interactions. Our analysis indicates that the observed Raver1-PTB interaction is a general mode of binding that applies to Raver1 complexes with PTB paralogues such as nPTB and to complexes of Raver2 with PTB.

INTRODUCTION

Alternative splicing in metazoans produces multiple mRNA transcripts from a single gene and is a powerful mechanism for amplifying proteome complexity. Over 95% of human multi-exon genes have multiple splice isoforms (Nilsen and Graveley, 2010). The process of pre-mRNA splicing involves the controlled inclusion or exclusion of specific exons and is regulated by cis-acting enhancer or silencer sequences found either within the exon or within the flanking introns (Matlin et al., 2005). The temporal and spatial control of splicing is also determined by various positive and negative protein co-factors, which are activated by developmental or differentiation-specific cues.

One of the most intensively studied regulators of alternative splicing is the polypyrimidine tract binding protein (PTB). PTB is a versatile protein. In addition to its nuclear splicing activity PTB is also found in the cytoplasm where it has roles in the stabilisation and localization of mRNA (Ghetti et al., 1992; Cote et al., 1999; Tillmar et al., 2002); it is also recruited to stimulate translation initiation driven by internal ribosome entry sites (IRES) from cellular and viral mRNAs (Sawicka et al., 2008).

PTB is expressed in a variety of tissues (Patton et al., 1991) and represses many muscle and neuron-specific exons, tissues in which PTB levels are low (Xue et al., 2009; Llorian et al., 2010). It has a number of tissue-specific paralogues in neurons (nPTB) (Markovtsov et al., 2000; Polydorides et al., 2000), hematopoietic cells (ROD1) (Yamamoto et al., 1999) and smooth muscle cells (smPTB) (Gooding et al., 2003) which, with at least 50% amino acid sequence identity, are closely related to the prototypical protein. These paralogues appear to supplant or modulate the program of splicing activity of PTB in the tissues where they occur (Boutz et al., 2007; Makeyev et al., 2007).

Though best known as a negative regulator of splicing, acting to exclude specific exons, PTB has recently been found to determine exon inclusion in some cases (Xue et al., 2009; Llorian et al., 2010). In common with a number of other splicing regulators, its activity appears to be determined by the location at which it binds to the RNA relative to the regulated exon (Witten and Ule, 2011).

Several different mechanisms have been proposed for the repressive splicing activity of PTB, including direct binding to pre-mRNA in order to block binding of U2AF65 — a component of the spliceosome — to the polypyrimidine tract (Lin and Patton, 1995; Singh et al., 1995) or oligomeric assembly across exons to mask splice sites (Wagner and Garcia-Blanco, 2001). In other cases, PTB does not directly block splicing factor binding, but rather the formation of splicing complexes across exons or introns; these indirect mechanisms appear to result from the ability of PTB to re-model pre-mRNA by bringing distal regions of RNA into close proximity and so inducing looping (Chou et al., 2000; Izquierdo et al., 2005; Cherny et al., 2010) or, as has been shown more recently, by bridging non-productive association of pre-mRNA with stem-loop IV of U1 snRNA (Sharma et al., 2008; Sharma et al., 2011). These mechanisms may all operate, depending on the particular pre-mRNA being spliced, though part of the observed variety is likely a reflection of the technical difficulty of studying splicing at the molecular level.

Nevertheless, it is clear that PTB binds to both RNA and proteins during splicing. The protein binds pyrimidine-rich motifs within RNA (e.g. UCUU, CUCUCU), which are found in regulatory elements (Pérez et al., 1997; Ray et al., 2009) that may be structured (Clerte and Hall, 2009; Kafasla et al., 2009). PTB binds RNA via β-sheet surfaces on the four RNA recognition motif domains (RRMs; Fig. 1A) (Conte et al., 2000; Simpson et al., 2004; Oberstrass et al., 2005) that are arrayed in an elongated conformation (Petoukhov et al., 2006). This arrangement allows multi-point contacts with RNA targets that can re-model or stabilise RNA structures containing pyrimidine-rich motifs and offers a plausible basis for models of PTB-mediated repression that invoke looping of pre-mRNA (Oberstrass et al., 2005; Cherny et al., 2010; Lamichhane et al., 2010) or contacts between pre-mRNA and U1 snRNA (Sharma et al., 2011).

Splicing regulation by PTB or its paralogues also appears to involve interactions with other regulatory proteins including Nova-1 and Nova-2 (Polydorides et al., 2000), Raver1 (Gromak et al., 2003) and MRG15 (Luco et al., 2010). The best characterised of these is the PTB-Raver1 interaction which modulates splicing of α-tropomyosin (Tpm1). PTB acts to exclude the mutually exclusive exon 3 of Tpm1 in smooth muscle cells but not in other cells where PTB is expressed (Gooding et al., 1998). Overexpression of PTB has little effect on this splicing event, suggesting that it is not limiting. However, overexpression of Raver1 (Hüttelmaier et al., 2001) causes a large increase in exon skipping (Gromak et al., 2003).

Raver1, which is expressed in most tissue types, can be found not only in the nucleus but also the cytoplasm, where it interacts with cytoskeletal proteins (Hüttelmaier et al., 2001). The protein has three N-terminal RRMs — although only RRM1 has demonstrable, albeit weak, RNA-binding activity (Lee et al., 2009)

— and an extended Pro-rich C-terminus that contains 4 conserved PTB interacting motifs (PRIs) with the consensus sequence [S/G][I/L]LGxxP (Rideau et al., 2006) (Fig. 1A). These motifs, which are essential for Raver1 function, bind exclusively to the α-helical side of the PTB RRM2 opposite to the RNA-binding surface, a mode of interaction that permits formation of ternary PTB-RNA-Raver1 complexes. The initial analysis of PTB-Raver1 interactions showed that only PRIs 1 and 3 bind with relatively high affinity (Rideau et al., 2006). Raver2, which is a related protein of unknown function, has a similar domain structure to Raver1: three N-terminal RRMs and a Pro-rich C-terminus (Fig. 1A) (Kleinhenz et al., 2005). Although the C-terminus is the least well-conserved portion between the two proteins, Raver2 contains two PRI motifs that are very similar to the PRI1 and PRI3 motifs found in Raver1 and have been shown also to mediate binding to PTB (Henneberg et al., 2010).

The first structural analysis of the interaction of peptides containing Raver1 PRI sequences with PTB only yielded an NMR-restrained docking model since the affinity of purified PTB RRM2 for synthetic PRI3 peptides was too low for a full structure determination (Rideau et al., 2006). Although it provided valuable insights, this model is not precise enough to allow full dissection of the structural basis of binding of Raver1 PRIs to PTB. By fusing Raver1 PRIs as N-terminal extensions to PTB RRM2, we have now obtained crystal structures of PTB RRM2 complexed with Raver1 PRI3 and PRI4, which are high-affinity and low-affinity motifs respectively. In combination with mutagenesis, binding and splicing assays, these new structural data reveal a mode of PTB-Raver1 interaction that is applicable to PTB paralogues and other PRI-containing proteins and that places useful constraints on models of the joint action of PTB and Raver proteins.

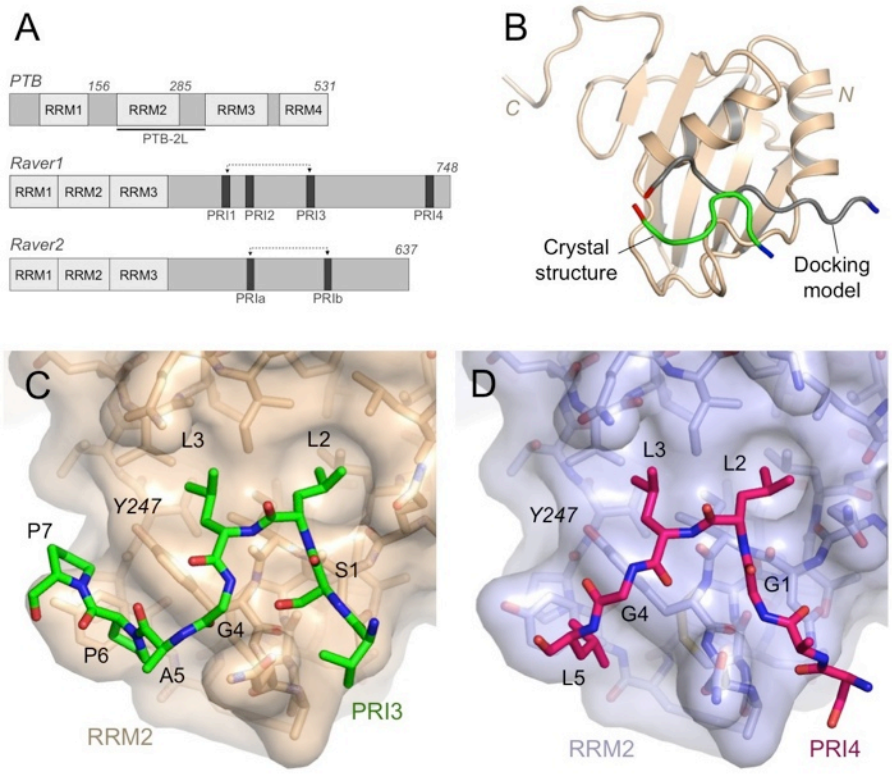

Figure 1. Structures of Raver1 PRIs bound to PTB RRM2.

(A) Schematic diagrams of PTB, Raver1 and Raver2 showing locations of RRMs and PRIs. Residue numbers are indicated above each protein.

(B) Comparison of the crystal structure of Raver1 PRI3 (green) bound to RRM2 (tan) with the NMR-restrained docking model of the PRI3 peptide (grey). The structures are shown schematically as cartoon representations; the N- and C-termini of the peptides are coloured blue and red respectively. Close up views of the interactions of (C and D) Raver1 PRI3 and Raver1 PRI4 with PTB RRM2. The Van der Waals surface of the RRM is depicted as a semi-transparent skin. All structural figures were created using PyMOL (Delano, 2002).

RESULTS

Construct design and characterization

To determine the structure of a PTB-Raver1 complex, we overcame the weak binding of short Raver1 peptides to PTB (Rideau et al., 2006) by fusing the PRI3 sequence as an N-terminal extension of PTB RRM2 to increase the local concentration artificially, a strategy that has worked for other protein-peptide complexes (Candel et al., 2007). The PTB-Raver1 docking model indicated that a linker of at least 20 amino acids would be required to join the C-terminal end of the bound PRI3 peptide to the N-terminus of RRM2 (Rideau et al., 2006). The first chimeric construct (PRI3-RRM2) was therefore designed to contain the 12-residue PRI3 sequence (PGVSLLGAPPKD — the conserved core residues, which we number 1-7, are underlined) followed by residues 156-285 of PTB RRM2. Residues 156-179 are from the polypeptide that links RRM1 to RRM2 in the full-length protein; residues 180-285 correspond to the structured RRM2 domain (Simpson et al., 2004) (see Experimental Procedures). The PRI3 sequence used in the chimera contains a Glu to Ala mutation at position 5 in the core sequence, a carry-over from the previous NMR analysis, but this substitution does not affect binding (Rideau et al., 2006).

The expression levels in E. coli and the solubility of the PRI3-RRM2 chimera are much higher than for constructs just containing RRM2 from PTB. PRI3-RRM2 is soluble to at least 25 mg/ml, whereas recombinant RRM2 precipitates above 6 mg/ml (Simpson et al., 2004). Although NMR analyses and size-exclusion chromatography suggested that PRI3-RRM2 exhibited concentration-dependent oligomerisation (not shown) the fusion protein produced diffraction-quality crystals. We therefore used the same strategy to fuse PRIs 1, 2 and 4 of Raver1 and the PRI from hnRNP-L and matrin-3 to PTB RRM2 (Fig. 3D). All these constructs had enhanced solubility similar to PRI3-RRM2, but only the construct containing the low-affinity PRI4 (SSEGLLGLGPGP) also crystallised.

Crystal structures of PRI3- and PRI4-RRM2

PRI3-RRM2 and PRI4-RRM2 crystals diffracted X-rays to 1.4 Å and 1.55 Å respectively. Diffraction data were phased by molecular replacement using the NMR structure of PTB RRM2 (Simpson et al., 2004) as a search model. In each case, only central portions of the PRI sequences were revealed by difference electron density maps (PRI3: VSLLGAPP; PRI4: SEGLLGL) (Fig. S1); there was no density for the linker peptides connecting these to the RRM2 domain so these were not incorporated into the atomic models. Final models for PRI3-RRM2 and PRI4-RRM2 were refined to R_{free} values of 23.1% and 22.1% respectively (see Table 1 for full statistics).

The crystals of PRI3-RRM2 and PRI4-RRM2 have 2 complexes in the asymmetric unit, which have almost identical structures: e.g. for PRI3-RRM2 the all atom RMSD is 0.22 Å (Fig. S1B). Comparison of the RRM2 structures in each complex with the solution structures of PTB RRM2 (RMSD=1.0 Å over C_α atoms) (Simpson et al., 2004; Oberstrass et al., 2005) reveals no significant structural changes upon peptide binding.

Conformations of PRI3 and PRI4 bound to PTB RRM2

The crystal structures of PRI3 and PRI4 from Raver1 in complex with PTB RRM2 are consistent with many of the features found in previous work: the peptides bind to the dorsal helical face of the RRM domain and in the same orientation as determined by NMR methods (Fig. 1B) (Rideau et al., 2006). However, they provide a much more detailed information on the peptide-RRM interaction and reveal previously undetected features of the bound peptide. Strikingly, although our NMR-restrained docking model assumed an extended conformation of the bound peptide, the core peptides of PRI3 and PRI4 in the crystal structures adopt S-shaped conformations that wrap around the peptide binding surface on RRM2, which is formed by the α1 and α2 helices plus the β1- α1 and α2- β4 loops (Fig. 1C,D). Our earlier NMR docking model for the Raver1-RRM2 complex was derived from eleven intermolecular NOEs involving methyl groups and aromatic rings (Rideau et al., 2006). All NOEs to Raver methyl groups are satisfied by the crystal structure presented here, with the exception of the A503, which is slightly farther away from the RRM domain than in solution (Figure S2). This small difference is not unexpected, as extensive conformational exchange was observed in NMR spectra of bound Raver1, and likely reflects some averaging in this region in solution.

There is an extensive bipartite hydrophobic interface between the peptides and RRM2: the pair of Leu side chains at positions 2 and 3 in the motif both project into a shallow apolar depression between the two helices on the dorsal face of RRM2, while downstream residues of the PRIs are packed around the side chains of Tyr 247 and Tyr 193, though in very different conformations for the two peptides (Fig. 2). For PRI3 the four-residue sequence ^{3}LGAP^{6} wraps around Tyr 247 (Fig. 2B), while in PRI4 a different backbone conformation means that just three residues, ^{3}LGL^{5}, are in contact with the tyrosine (Fig. 2D). Moreover, although in PRI3 Pro 6 and Pro 7 both contact the side chains of Tyr 247 and Tyr 193, the equivalent residues in PRI4 (Gly 6 and Pro 7) are not visible in the electron density map, presumably due to disorder; this difference is likely to contribute to the lower affinity of PRI4. The occlusion of hydrophobic features on the surface of RRM2 by the Raver1 peptide probably accounts for the enhanced solubility of the chimeric PRI-RRM2 proteins.

Table 1. Data collection, Data processing and refinement statistics for crystal structures of PRI3-RRM2 and PRI4-RRM2.

	PRI3-RRM2	PRI4-RRM2
Refinement Statistics		
Space Group	C2	C2
a, b, c (Å)	74.23, 60.60, 60.84	74.48, 60.38, 61.06
α, β, γ (°)	90, 90, 107.51	90, 90, 107.86
Resolution Range (Å)	30.32-1.40 (1.48-1.40)	35.49-1.55 (1.63-1.55)
Reflections	50129	36156
Multiplicity	5.6 (5.3)	2.4 (2.4)
Completeness (%)	98.9 (96.1)	96.9 (96.5)
I/σ_I	15.4 (5.3)	10.2 (3.0)
R_{merge} (%)	6.4 (35.4)	5.5 (35.8)
Refinement Statistics		
R_{calc} (%)	22.3	21.6
R_{free} (%)	23.1	22.1
Non-hydrogen atoms	1741	1723
Waters	191	132
rms bond lengths (Å)	0.005	0.005
rms bond angles (°)	1.32	1.31
Ramachandran (% favoured/allowed)	98.0/1.4	97.7/2.3
PDB ID	3zzy	3zzz

Values in parentheses are for the highest resolution shell. PDB, Protein Data Bank; rms, root-mean-square.

The observed hydrophobic contacts made by the Leu side-chains at positions 2 and 3 in the PRI explain why substitution of either residue by smaller apolar residues is detrimental to binding (Rideau et al., 2006). However, it is not clear why a Leu-to-Ile substitution at position 2 in PRI3 has no effect, whereas the same substitution at position 3 effectively abrogates binding of the Raver1 PRI, especially since Leu 3 binds within a shallower depression. Perhaps the branching at the C_β in Ile introduces a steric clash that distorts nearby hydrogen bonds between the Raver1 PRI3 and PTB RRM2.

In addition to the apolar contacts, there are specific hydrogen bond interactions that contribute to PRI binding to PTB RRM2. These show clear differences between PRI3 and PRI4, which probably also contribute to the affinity differences between these two motifs. In PRI3 (core sequence: SLLGAPP) Leu 2 and Leu 3 both project in the same direction into the binding pocket on PTB RRM2 because of a pinched backbone conformation that is stabilised by an internal hydrogen bond from the side-chain hydroxyl of Ser 1 to the backbone amide of Gly 4 (Fig. 2A). In this conformation the peptide is able to make four hydrogen bonds to PTB RRM2.

In contrast, PRI4 (core sequence: GLLGLGP) makes only 3 intermolecular hydrogen bonds. The absence of Ser at position 1 eliminates the intra-peptide hydrogen bond and results in a more open backbone conformation. The loss of this internal interaction allows the peptide bond between Leu 3 and Gly 4 to flip with respect to PRI3, a conformational change that eliminates a hydrogen bond to RRM2 (from the carbonyl group of Gly 4 –Fig. 2C), which likely reduces the affinity of this motif, although the peptide flip is also needed to allow the ^{3}LGL^{5} sequence to wrap around Tyr 247.

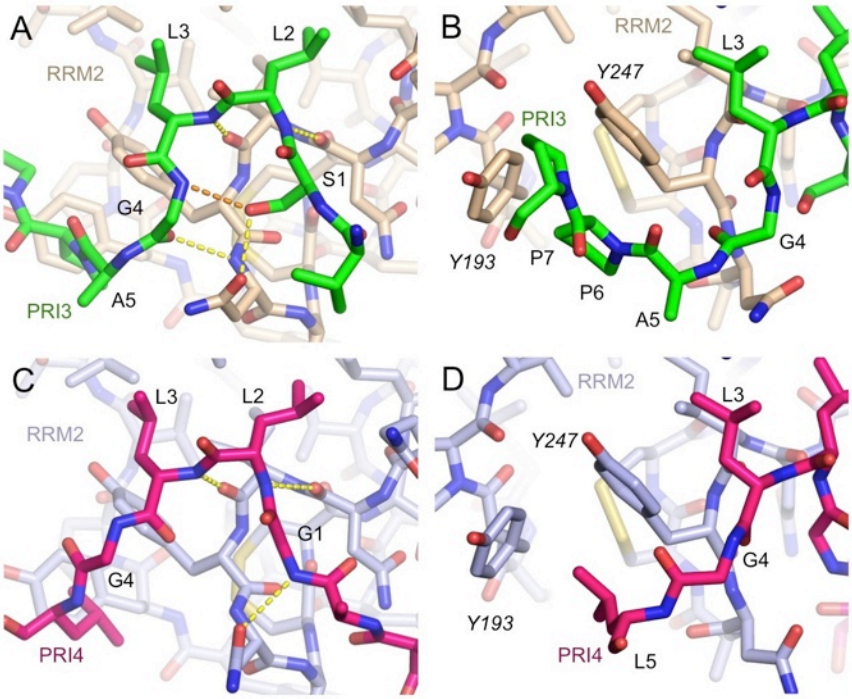

Figure 2. Detailed structural comparison of Raver 1 PRIs 3 and 4 bound to PTB RRM2.

(A, B) Close up views of PRI3 bound to RRM2. Intramolecular hydrogen bonds are shown as orange dashes; intermolecular hydrogen bonds are yellow. (C, D) Equivalent views of PRI4 bound to RRM2.

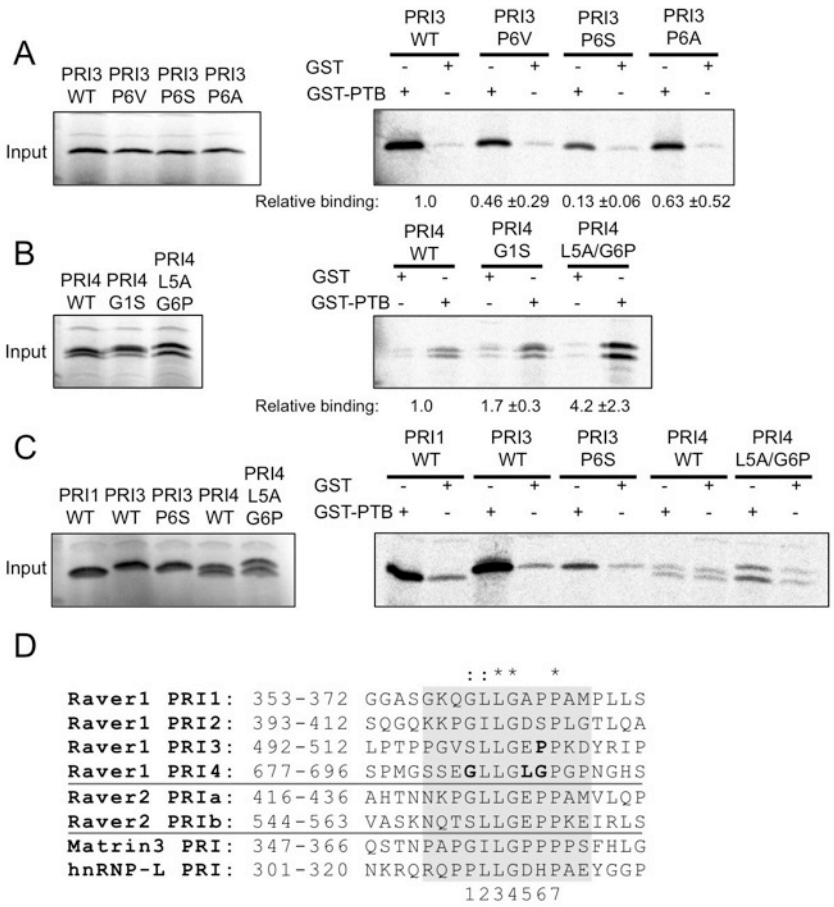

Figure 3. Effect of mutations of Raver1 PRIs on binding to GST-PTB.

(A) Pull-down assays of binding of Raver1 PRI3 mutants to GST-PTB. Left Loading controls for ^{35}S-Met-labelled PRI3-MS2 fusion proteins containing PRI3 wt and the mutants P6V, P6S and P6A (Experimental Procedures). Right, Autoradiogram of PRI3-MS2 proteins pulled down with GST (1 μg) or GST-PTB (3 μg).

(B)Pull-down assays of binding of Raver1 PRI4 mutants to GST-PTB. Left Loading controls for ^{35}S-Met-labelled PRI4-MS2 fusion proteins. Right, GST Pull-down of PRI4 constructs with GST (5 μg) or GST-PTB (15 μg). Although PRI4 constructs migrate as a doublet (as observed previously (Rideau et al., 2006)), both products of the in vitro transcription-translation reaction contain the PRI since they bind PTB with the same affinity.

(C)Comparison of binding of wild-type and mutant Raver1 PRIs to GST-PTB. Left Loading controls. Right, GST Pull-down of PRI4 constructs with GST (2 μg) or GST-PTB (6 μg).

(D) PRI sequences from murine Raver1 (AAP33691), murine Raver2 (NP_898845), human matrin-3 (NP_001181884) and human hnRNP-L (NM_001533). Sequences shown for Raver1 are the 20 amino peptides used in pull-down assays; the shaded box indicates the sequences included in PRI-RRM2 chimeras for structural studies. Sequence similarity and identity within the PRI core are indicated. Residues in Raver1 PRIs 3 and 4 that were tested by mutagenesis are in boldface.

Dissecting the structural basis of differential PRI affinity

Previous work established that PRIs 1 and 3 bind with significantly higher affinity than PRIs 2 and 4 (Rideau et al., 2006). The new structural information suggests that the Leu 2-Leu 3 dipeptide found in both motifs is not sufficient for high-affinity binding; instead variations in amino acids at positions 1, 5 and 6 appear to be crucial. To explore this idea we introduced mutations into PRI3 and PRI4 peptides (fused to MS2 proteins at their C-termini) and tested their effect on binding affinity in pull-down assays (Experimental Procedures).

Pro 6 of PRI3, which is conserved in the other high affinity motif, PRI1, makes apolar contacts with Tyr 247 and Tyr 193 that are likely to contribute significantly to binding affinity. This was confirmed by mutagenesis: although conservative mutations of Pro 6 to Ala or Val, both of which retain the apolar character of the side chain, only very slightly reduced the affinity of PRI3 for PTB RRM2, substitution by a polar Ser reduced binding 7-fold (Fig. 3A). Thus, the presence of a polar residue at position 6 within the PRI is detrimental to binding, a result that is consistent with the low-affinity of Raver1 PRI2 and the PRI from hnRNP L, which have Ser and His at this position respectively (Rideau et al., 2006) (Fig. 3D).

To further explore the peptide features that affect binding to PTB, we performed experiments to examine what changes would be necessary to enhance the binding affinity of Raver1 PRI4. The structure shows that the presence of Gly 1 in PRI4 eliminates the internal stabilisation of the backbone of PRI3 due to the hydrogen bond between Ser 1 and Gly 4 (Fig. 2 A & C). However, this interaction seems to have little effect on the affinity for RRM2 since substitution of Gly 1 by Ser in PRI4 only increased the binding 1.7-fold (Fig. 3B), consistent with the observation that Gly occurs at position 1 in the high affinity PRI1 sequence (Fig. 3D). In contrast, there was a stronger 4 -fold enhancement of binding when the double mutation Leu5Ala/Gly6Pro was used to convert the ^{3}LGLGP^{7} sequence in PRI4 to the ^{3}LGAPP^{7} found in our modified version of the high-affinity PRI3 and in PRI1 (Fig. 3B). Together these observations suggest that interaction of Pro 6 with the tyrosine pocket in PTB RRM2 is essential for a high-affinity interaction with PTB, while the backbone stabilisation due to Ser 1 plays a minor supporting role. Moreover, the mutagenesis results help to verify the functional relevance of the structures obtained from our artificial chimeric constructs.

Intriguingly, the L5A/G6P substitutions in PRI4 make its core sequence identical to that of PRI1 (Fig. 3D) but this mutant binds about 10-fold less well to GST-PTB than PRI1 (Fig. 3C). This suggests that elements outside the conserved core motif of Raver1 may play a role in binding to PTB. However, although the 20-residue peptide sequence used in the binding assays is longer than the 12-residue sequence incorporated into the chimeric constructs used for crystallisation, comparison of the flanking sequences (Fig. 3D) reveals no obvious patterns of conservation that correlate with binding.

Interactions of Raver1 PRIs with nPTB

To identify whether the mode of binding of Raver1 PRI peptides to PTB is the same in other PTB paralogues, we investigated their binding to GST-nPTB in pull-down assays. The sequence identity between PTB and nPTB is over 74% (Markovtsov et al., 2000; Polydorides et al., 2000). Mapping of the RRM2 sequence differences between PTB and nPTB onto the structure reveals that they cluster in 2 distinct regions. One group is located on the upper surface of helix α2, quite separate from the PRI binding site, whereas a second smaller cluster occurs on the β1-α1 loop which, together with the adjacent α2-β4 loop, forms part of the Raver1 binding surface (Fig. S3A). Despite these differences, binding assays revealed that the relative affinities of PRIs 1-4 for PTB and nPTB are very similar. Thus, PRI1 and PRI3 bind strongly to both paralogues, while PRI2 and PRI4 have much weaker affinity (Fig. S3C). Furthermore, mutations designed to reduce or enhance the affinities of PRI3 and PRI4 for PTB RRM2

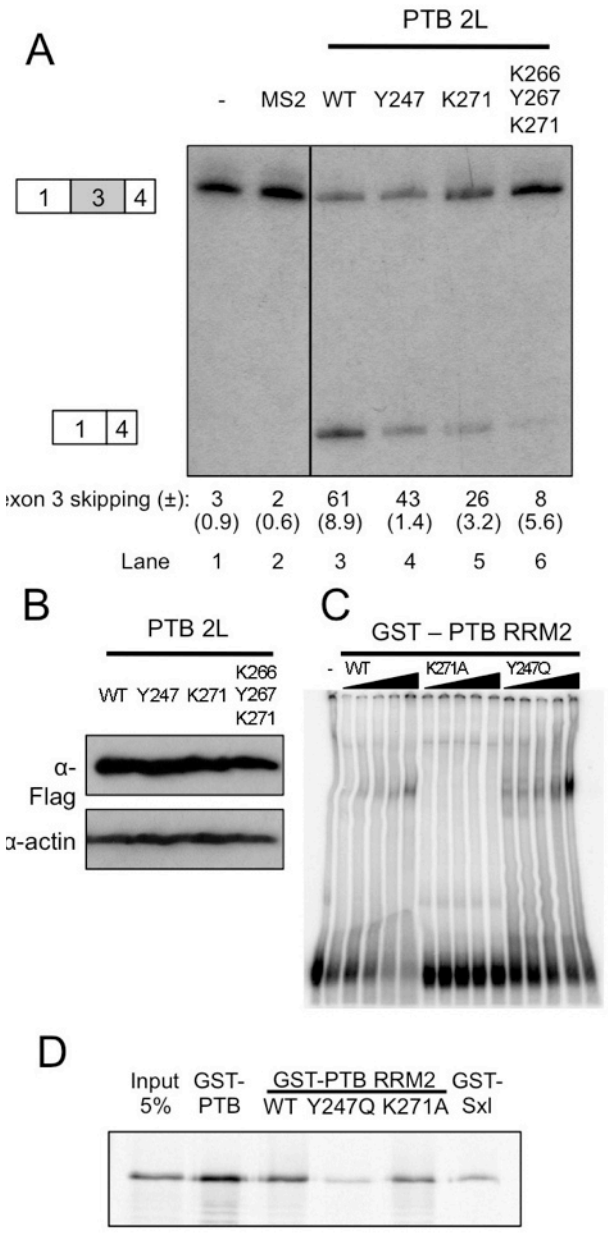

Figure 4. Mutation of PTB RRM2 RNA and PRI interacting surfaces impairs activity.

(A) Effects of RRM2 mutations on an MS2-tethered splicing regulation assay. The Tpm1 exon 1-3-4 splicing reporter, with the PTB site downstream of exon 3 replaced by a pair of MS2 coat protein binding sites, was transfected into HeLa cells and splicing patterns analyzed by RT-PCR. Lane 1, reporter alone, lane 2, cotransfected with MS2 coat protein. Lanes 3-6 reporter cotransfected with MS2-PTB2L expression constructs (wt, Y247Q, K271A, K266A/Y267A/K271A, respectively). Percent exon skipping (± sd) is shown below each lane.

(B) Western blots to show equivalence of expression of MS2-PTB2L tested in panel A (anti-FLAG). Loading control, anti-actin.

(C) Electrophoretic mobility shift assay of 0.23.2 μM recombinant PTB RRM2 wild type (lanes 2-6), Y247Q (lanes 7-11); K271A. Lane 1, no protein.

(D) Pull-down of in vitro translated full length Raver1 with the indicated GST-fusion proteins.

had similar effects on their binding to nPTB: the P6S mutation in PRI3 P6S reduced binding for nPTB, while the binding PRI4 L5A/G6P was enhanced (compare Fig. S3C with Fig. 3). These observations support the contention that PTB and nPTB interact with Raver1 PRIs in the same way.

PTB mutations affect PRI binding and activity

To extend our understanding of the PTB-Raver1 interaction we generated PTB RRM2 mutants and tested them for binding of Raver1 and RNA and for their ability to regulate splicing of Tpm1.

PTB RRM2, along with the following inter-RRM linker (PTB 2L), was previously shown to be fully active as a splicing repressor domain when fused to MS2 coat protein and tethered to Tpm1 RNA by an MS2 binding site, which replaced the natural downstream PTB binding site (Robinson and Smith, 2006). We therefore used this tethered repressor domain assay to test the effects of mutations designed to target the PTB-Raver1 interaction. Cotransfection of the splicing reporter construct with an MS2 expression vector had no effect on the low basal level of exon skipping (Fig. 4A lanes 1,2), while transfection of wild type PTB 2L-MS2 led to 61% exon skipping (lane 3). Mutations of Tyr 193, Leu 241 and Gln 244 had no effect (data not shown). However, mutation of Tyr 247 to Gln reduced activity by a third (Fig. 4A, lane 4). This reduction in activity is consistent with the close contacts made by Tyr 247 with hydrophobic side chains in each of the PRIs (Fig. 2B,D). As a control, we also tested the effects of mutations on the RNA binding surface of RRM2 (K271A and K266A/Y267A/K271A), which are predicted to have no effect on PRI binding. Both single and triple RNA binding mutations severely impaired the splicing repressor activity (Fig. 4A, B). To confirm the specificity of the mutations, recombinant GST-PTB RRM2 proteins were tested for the ability to pull-down in vitro translated Raver1 protein (Fig. 4D) and to bind to RNA (Fig. 4C). As expected, the Y247Q mutant showed complete impairment of Raver1 interaction (Fig. 4D; compare to GST-Sxl non-specific control), but bound to RNA comparably to wild-type RRM2. In contrast, the K271A mutant was impaired for RNA binding but interacted with Raver1. These observations are consistent with the previous finding that PTB RRM2 can form a ternary complex with the Raver1 PRI and a short RNA oligomer (Rideau et al., 2006), and confirm the independence of the two interacting surfaces of RRM2. Moreover, it is interesting to note that, given that RRMs 1 and 2 of PTB have been shown to interact with U1 stem-loop 4 (Sharma et al., 2011), the strong effect of the RNA binding mutations in PTB 2L-MS2 on repression of Tpm1 exon 3 (Fig. 4) may be due to impairment of binding to U1 snRNA.

DISCUSSION

In this report we present the first structural analysis of a PTB-protein complex involved in splicing: the crystal structures of PTB RRM2 in complex with two peptide motifs from Raver1, the protein recruited to co-repress exon 3 of Tpm1. Though the structures contains only a single domain of PTB, this is the major structured portion of PTB-2L, the minimal fragment required to recapitulate the activity of the full-length protein in exon exclusion (Robinson and Smith, 2006) and, as has been shown more recently, inclusion (Xue et al., 2009; Llorian et al., 2010).

Analysis of the structure and RNA-binding properties of PTB have helped to inform ideas about how PTB works, first by delineating the unexpected architecture of the domains and so paving the way for more precise functional studies using structure-based mutagenesis (Conte et al., 2000; Simpson et al., 2004; Oberstrass et al., 2005), and then by revealing modes of RNA binding, which led to testable suggestions of how binding of PTB might re-model RNA to affect splicing (Oberstrass et al., 2005; Petoukhov et al., 2006; Lamichhane et al., 2010).

Our growing understanding of PTB-RNA interactions has influenced models of PTB-mediated exon repression — its best-characterised activity. Several plausible mechanisms have emerged, built on the observation that PTB molecules are involved at multiple binding sites in pre-mRNA located within or near to regulated exons. Possible modes of repression include masking of splicing signals by direct contact (Singh et al., 1995; Wagner and Garcia-Blanco, 2001) or PTB-mediated looping (Chou et al., 2000; Oberstrass et al., 2005; Cherny et al., 2010; Lamichhane et al., 2010; Llorian et al., 2010); additionally or alternatively PTB may interfere with spliceosome assembly by binding to stem-loop 4 of U1 snRNA (Sharma et al., 2011).

Less attention has been paid to the interactions that PTB makes with other proteins to regulate splicing (or indeed, any

other PTB-mediated activity), despite observations of PTB-binding partners that have accumulated over the past ten years and now include not only Raver1 and Raver2 (Hüttelmaier et al., 2001; Henneberg et al., 2010), but also Nova-1/2 (Polydorides et al., 2000) and, possibly, MRG15 (Luco et al., 2010). Clearly delineation of the details of PTB-protein interactions is important for a more complete understanding of the molecular mechanism of splicing regulation.

The crystal structures of PTB RRM2 in complex with Raver1 reveals a mode of peptide binding that has been observed in other RRM-peptide complexes such as U2AF35/U2AF65 (Kielkopf et al., 2001), SPF45/SF3b155 (Corsini et al., 2007) and eIF3b/eIF3j (Elantak et al., 2010): the peptide binds in an orientation that is broadly perpendicular to the two helices on the dorsal surface of the RRM (Fig. 5). [The REF/ICP27 complex, in which the peptide lies parallel to the helices, is a notable exception (Tunnicliffe et al., 2011) (Fig. S4)].

Nevertheless, the PTB-Raver1 complex marks an interesting variation on this theme. Although in the three examples of perpendicular binding mentioned above peptide binding is anchored by insertion of a Trp side-chain from the peptide into a deep apolar pocket between the helices on the RRM, in the Raver1 peptide the role of this Trp is taken by a pair of Leu side-chains that insert into a shallower hydrophobic depression in a similar location on the RRM. This pair of Leu side-chains make important hydrophobic contacts that contribute to binding of Raver1 PRIs to PTB RRM2, but they are not sufficient for high-affinity binding since this sequence feature is also found in PRIs 2 and 4, which have lower affinity (Rideau et al., 2006). Additional interactions are also important for tight binding. The PRI3-RRM2 complex reveals that these include a number of specific hydrogen bonds — mostly between main-chain groups — and the interaction of the Pro-Pro dipeptide at positions 6 and 7 in the motif with the Tyr pocket formed by Tyr 247 and Tyr 193 (Fig. 2B). Although PRI4 exhibits an alternative mode of binding, which inserts a hydrophobic Leu side-chain (from position 5 of the motif) within this Tyr pocket, this is insufficient for high-affinity binding (Fig. 3C). Moreover, mutagenesis experiments show that substitution of the Pro at position 6 in the PRI3 motif with a polar residue (such as Ser) is sufficient to impair binding (Fig. 3A), a result that accounts for the low affinity observed for the PRI2 sequence of Raver1 (Rideau et al., 2006). The overall mix of interactions observed echoes similar observations from other structures of RRM-peptide complexes such as U2AF35/U2AF65 (Kielkopf et al., 2001), and SPF45/SF3b155 (Corsini et al., 2007).

Given the close sequence similarity between the PRI1 and PRI3 motifs from Raver1, the structural and binding data presented here offer a plausible explanation for the high affinity of PRI1 and strongly suggest it binds to PTB RRM2 in the same way. The same can probably also be said of the two high-affinity PRI motifs in Raver2 which are similar to Raver1 PRI1 and PRI3 (Henneberg et al., 2010) (Fig. 3D).

We have also shown that despite a cluster of sequence differences between PTB and its neuronal paralogue near the Raver1-binding site on RRM2, nPTB exhibits a very similar pattern of variation of affinity for the Raver1 PRIs (Fig. S3). The Raver1 binding site is

therefore common to both these paralogues and it will be worth investigating whether this function is retained by other PTB paralogues such as ROD1 (Yamamoto et al., 1999; Hüttelmaier et al., 2001) and smPTB (Gooding et al., 2003).

Furthermore the results allow us to refine the definition of what constitutes a high-affinity PRI sequence from [S/G][I/L]LGxxP to [S/G][I/L]LGxΦP, where the Φ at position 6 indicates a preference for a small hydrophobic residue (Pro, Val, Ala). Using ScanProsite (de Castro et al., 2006) 36 human proteins can be identified that contain predicted high affinity PRIs conforming to ([S/G][I/L]LGx[AVP]P, including Raver1 and 2, each of which contain two sites. The nuclear matrix protein matrin-3 contains the motif GILGPPP, which is necessary and sufficient for interaction with PTB (M.C. and C.W.J.S. manuscript in preparation). In addition, the 3´ end processing factors CSTF2 and CSTF2T both contain the motif GLLGDAP suggesting a molecular basis for how PTB is able to activate some polyadenylation sites (Castelo-Branco et al., 2004). Other potential PRI containing proteins such as the deacetylase HDAC6

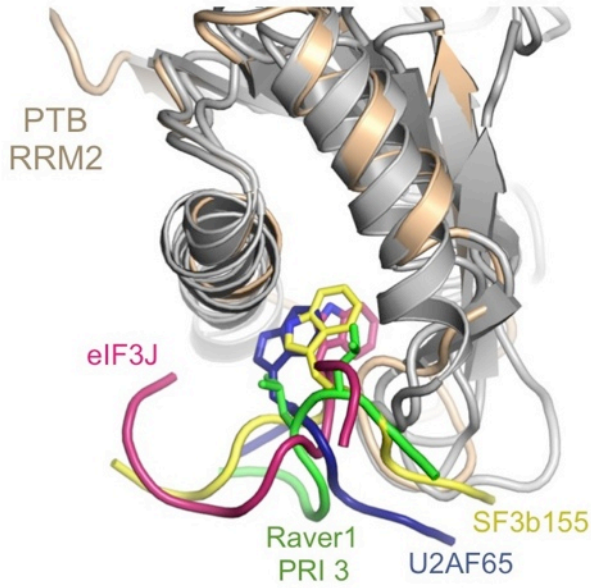

Figure 5. Comparison of the PTB-Raver1 interaction with other peptide-RRM complexes.

A common mode of binding is revealed by superposition of the complex of Raver1 PRI3 and PTB RRM2 with the peptide/RRM complexes of U2AF65/U2AF35 (PDB – 1jmt), SF3b155/SPF45 (PDB - 2peh) and eIF3j/eIF3b (PDB – 2krb). PTB RRM2 is coloured tan; other RRMs are grey. The superposition was performed for the RRM domains using PyMOL (Delano, 2002).

and a histone demethylase, JMJD8, hint at further interesting and functionally diverse targets of PTB.

The PTB-Raver1 complexes presented here place constraints on possible modes of co-repression by PTB and Raver1. Although there are four PTB-binding motifs in the C-terminal region of Raver1, each appears capable of only binding to a single molecule of PTB. The stoichiometry of PTB-Raver1 complexes that assemble on regulated exons could therefore be 2:1, if only high-affinity sites are engaged. However, it remains possible that low affinity sites may also contribute to binding, not least because tethering of Raver1 to PTB via the two high-affinity sites will augment the local concentration of PRIs. This would be consistent with the model envisaged by Cherny and colleagues (2010), on the basis of their observations of multiple PTB molecules binding in the vicinity of regulated exons in Tpm1. Against this, however, it is has been observed that mutation of a single PRI3 motif in Raver1 — and of an identical PRI in Raver2 (PRIb in Fig. 3D) — was sufficient to abrogate binding to PTB and PTB-mediated localisation to perinucleolar comparments in HeLa (Henneberg et al., 2010). While this may point to a 1:1 stoichiometry for PTB-Raver1 complexes, it remains true that mutation of other high-affinity PRIs in Raver1 or Raver2 significantly reduces binding to PTB (Rideau et al., 2006; Henneberg et al., 2010). The full details of functional PTB-Raver1 interactions have yet to be worked out. It is tantalising to note the similar spacing between the high-affinity PRIs in Raver1 and Raver2 (about 135 amino acids; see Fig. 1A), which perhaps points to a common architecture of functional PTB-Raver complexes.

EXPERIMENTAL PROCEDURES

Plasmid construction

For structural analysis PRI-RRM2 chimera constructs containing residues 156-285 of PTB were generated by PCR using PTB1 cDNA as a template (Gil et al., 1991). The forward primer incorporated an NcoI site and sequences coding for 12 amino acids from the PRI sequences (from Raver1, hnRNP-L and matrin-3), while the reverse primer introduced a stop codon and downstream HindIII site. The resulting PCR product was ligated into the pETM-11 vector, which adds a TEV^{pro}-cleavable N-terminal 6xHis tag (Zou et al., 2003).

For pull-down experiments we used Quikchange (Stratagene) to mutate MS2-Raver1 fusion proteins that were made previously (Rideau et al., 2006). These incorporate 20-residue Raver1 PRI sequences as N-terminal extensions. Plasmids for GST-PTB (Gromak et al., 2003) and GST-nPTB — a gift from B.J. Blencowe — (Calarco et al., 2009) have been described. All plasmids were sequenced by MWG Eurofins Ltd.

Protein expression and purification

PTB proteins were expressed at 37°C in E. coli BL21 (DE3). Cell pellets were lysed by sonication in Buffer A (250 mM NaCl, 25 mM Tris, pH 7.8), 0.1% (v/v) Triton X-100 and 0.5 mM phenylmethanesulfonylfluoride containing 1 mg/ml lysozyme. 6xHis tagged proteins were purified from clarified lysates using TALON resin (Clontech). Purified proteins eluted in Buffer A containing 100 mM imidazole. The 6xHis tag was removed by overnight incubation at 4°C with 1 mg of his-tagged TEV^{pro} per 30 mg of PRI-RRM2 during dialysis against Buffer A with 5 mM β-mercaptoethanol. The cleaved tag and TEV^{pro} were removed in a second round of TALON purification. For crystallization, proteins were further purified by gel filtration on a Superdex 75 16/60 column (GE Healthcare) in 100 mM NaCl, 25 mM Tris (pH 7.8) and 1 mM dithiothreitol (DTT).

For pull-down assays to monitor Raver1 binding, Glutathione S-transferase (GST) tagged PTB proteins were extracted from E. coli in a similar manner and applied a glutathione sepharose 4B column (GE Healthcare). The column was washed with Buffer A and proteins eluted in Buffer A + 5 mM DTT and 20 mM glutathione (pH 9.0). Purified proteins were concentrated by centrifugal filtration to 22 mg/ml, 28 mg/ml, 5.5 mg/ml and 4.3 mg/ml for PRI3-RRM2, PRI4-RRM2, GST-PTB and GST-nPTB respectively and stored at -80°C.

GST-PTB RRM2 fusion proteins used in Fig. 4 were PCR amplified and cloned into the EcoRI site in pGEX3 (to incorporate residues 181-284). Cells were lysed by passing twice through a French press in MTPBS buffer (150 mM NaCl, 16 mM NaH_2PO_4, 1 mM DTT, 3 mM PMSF, EDTA-free protease cocktail (Roche)). Soluble and insoluble fractions were separated by centrifugation at 8,000g for 10min. GST fusion proteins were purified through a glutathione sepharose 4B column (GE Healthcare), washed with MTPBS+1% Triton X-100, and step-eluted using reduced glutathione. Protein containing fractions were dialyzed in buffer E (20mM Hepes, 100mM KCl, 3mM MgCl2, 0.1mM EDTA, 1mM DTT, 20% glycerol, 0.05% NP-40). The GST-PTB and GST-SXL proteins used as control in Fig. 4D were prepared as described (Rideau et al, 2006).

Structure Determination

Purified recombinant PRI-RRM2 proteins at ~18 mg/ml were crystallized by sitting drop vapour diffusion using a reservoir solution containing 0.2 M NaI, 0.1 M Bis-Trispropane (pH 6.5) and 20% polyethylene glycol 3350. Crystals were soaked for 1 min in mother liquor with 20% glycerol before flash freezing in liquid N_2. X-ray diffraction data were collected at beamlines X13 at DESY, Hamburg, Germany and I02 at Diamond Light Source, Didcot, UK. The data were processed with iMosflm and scaled using SCALA from the CCP4 suite (Collaborative Computer Project No. 4, 1994). PRI3-RRM2 data were phased by molecular replacement in Phaser v1.2 (McCoy et al., 2007) using the ensemble of NMR structures of PTB RRM2 as a search model (Simpson et al., 2004). PRI4-RRM2 was phased by rigid body refinement using the RRM2 domain from the refined PRI3-RRM2 structure since the two chimeric proteins crystallised isomorphously. Models were manually adjusted in O (Jones et al., 1991) and refined with CNS (Brunger et al., 1998).

Pull-down assays

In vitro GST pull-down assays were performed essentially as described in (Gromak et al., 2003). Briefly, ^{35}S-Met labelled MS2-Raver1 proteins produced by in vitro transcription-translation reactions (TNT quick coupled system, Promega) were incubated for 3 hours at 4°C with GST, GST-PTB or GST-nPTB in wash buffer (100 mM KCl, 20 mM HEPES (pH 7.9), 0.5 mM DTT, 0.2% Tween-20 and 10% glycerol) in the presence of 5 µL glutathione sepharose 4B. Beads were then washed three times with wash buffer and bound protein eluted using SDS loading buffer for SDS-PAGE analysis. Protein band intensities on dried gels were recorded using a Fuji FLA-5000 phosphor imager; quantitative densitometry was performed using AIDA software (Raytest).

Electrophoretic mobility shift assays (EMSAs)

GST-PTB RRM2 proteins (0.2-3.2 µM) were incubated with 10 fmol of an RNA probe spanning the Tpm1 exon 3 polypyrimidine tract which is enriched in PTB binding sites (Cherny et al., 2010) in 10mM Hepes, 100mM KCl, 3mM MgCl2, 5% glycerol, 1mM DTT, 0.25 µg of E. coli rRNA, RNase inhibitor (DCP) for 30 min at 30ºC and loaded directly onto a 5% polyacrylamide (40:1) gel.

Splicing assays

Splicing transfection assays were carried out as before (Robinson & Smith, 2006). Briefly 200 ng of the splicing reporter and 800 ng of effector DNA were transfected into HeLa cells in 35mm wells, followed by RT-PCR analysis of the splicing products 48 hours after transfection(Robinson and Smith, 2006). The splicing reporter pT2Δbp-2MS2 is a modified version of TM-2MS2 (Robinson and Smith, 2006) containing a mutation of the canonical branch-point of the Tpm1 exon 3, which leads to enhanced exon skipping in HeLa cells (Gooding et al., 2006).

Acknowledgements

This work was funded by grant support from the BBSRC (BB/E002209X) and the Wellcome Trust (092900). AJ is grateful for the award of a Doctoral Training Award from the BBSRC. MBC was supported by a PhD studentship from the Portuguese Foundation for Science and Technology (SFRH/BD/15898/2005). We thank the staff at EMBL DESY (Germany) and the Diamond Light Source (UK) for help with data collection, and Ben Maddox and Clare Gooding for constructing the PTB RRM2 mutants.

REFERENCES

Boutz, P.L., Stoilov, P., Li, Q., Lin, C.H., Chawla, G., Ostrow, K., Shiue, L., Ares, M., Jr., and Black, D.L. (2007). A post-transcriptional regulatory switch in polypyrimidine tract-binding proteins reprograms alternative splicing in developing neurons. Genes Dev. 21, 1636-1652.

Brunger, A.T., Adams, P.D., Clore, G.M., DeLano, W.L., Gros, P., Grosse-Kunstleve, R.W., Jiang, J.S., Kuszewski, J., Nilges, M., Pannu, N.S., et al. (1998). Crystallography & NMR system: A new software suite for macromolecular structure determination. Acta Crystallogr. D54, 905-921.

Calarco, J.A., Superina, S., O'Hanlon, D., Gabut, M., Raj, B., Pan, Q., Skalska, U., Clarke, L., Gelinas, D., van der Kooy, D., et al. (2009). Regulation of vertebrate nervous system alternative splicing and development by an SR-related protein. Cell 138, 898-910.

Candel, A.M., Conejero-Lara, F., Martinez, J.C., van Nuland, N.A.J., and Bruix, M. (2007). The high-resolution NMR structure of a single-chain chimeric protein mimicking a SH3-peptide complex. FEBS Lett. 581, 687-692.

Castelo-Branco, P., Furger, A., Wollerton, M., Smith, C., Moreira, A., and Proudfoot, N. (2004). Polypyrimidine tract binding protein modulates efficiency of polyadenylation. Mol. Cell. Biol. 24, 4174-4183.

Cherny, D., Gooding, C., Eperon, G.E., Coelho, M.B., Bagshaw, C.R., Smith, C.W.J., and Eperon, I.C. (2010). Stoichiometry of a regulatory splicing complex revealed by single-molecule analyses. EMBO J. 29, 2161-2172.

Chou, M.Y., Underwood, J.G., Nikolic, J., Luu, M.H., and Black, D.L. (2000). Multisite RNA binding and release of polypyrimidine tract binding protein during the regulation of c-src neural-specific splicing. Mol. Cell 5, 949-957.

Clerte, C., and Hall, K. (2009). The Domains of Polypyrimidine Tract Binding Protein Have Distinct RNA Structural Preferences. Biochemistry 48, 2063-2074.

Collaborative Computer Project No. 4 (1994). The CCP4 suite: programs for protein crystallography. Acta Crystallogr. D50, 760-763.

Conte, M.R., Grüne, T., Ghuman, J., Kelly, G., Ladas, A., Matthews, S., and Curry, S. (2000). Structure of tandem RNA recognition motifs from polypyrimidine tract binding protein reveals novel features of the RRM fold. EMBO J. 19, 3132-3141.

Corsini, L., Bonnal, S., Bonna, S., Basquin, J., Hothorn, M., Scheffzek, K., Valcárcel, J., and Sattler, M. (2007). U2AF-homology motif interactions are required for alternative splicing regulation by SPF45. Nat. Struct. Mol. Biol. 14, 620-629.

Cote, C.A., Gautreau, D., Denegre, J.M., Kress, T.L., Terry, N.A., and Mowry, K.L. (1999). A Xenopus protein related to hnRNP I has a role in cytoplasmic RNA localization. Mol. Cell 4, 431-437.

de Castro, E., Sigrist, C.J., Gattiker, A., Bulliard, V., Langendijk-Genevaux, P.S., Gasteiger, E., Bairoch, A., and Hulo, N. (2006). ScanProsite: detection of PROSITE signature matches and ProRule-associated functional and structural residues in proteins. Nucleic Acids Res. 34, W362-365.

Delano, W.L. (2002). The PyMOL molecular graphics system (San Carlos, CA, USA: DeLano Scientific).

Elantak, L., Wagner, S., Herrmannová, A., Karásková, M., Rutkai, E., Lukavsky, P.J., and Valásek, L. (2010). The indispensable N-terminal half of eIF3j/HCR1 cooperates with its structurally conserved binding partner eIF3b/PRT1-RRM and with eIF1A in stringent AUG selection. Journal of Molecular Biology 396, 1097-1116.

Ghetti, A., Piñol-Roma, S., Michael, W.M., Morandi, C., and Dreyfuss, G. (1992). hnRNP I, the polypyrimidine tract-binding protein: distinct nuclear localization and association with hnRNAs. Nucleic Acids Res. 20, 3671-3678.

Gil, A., Sharp, P.A., Jamison, S.F., and Garcia-Blanco, M.A. (1991). Characterization of cDNAs encoding the polypyrimidine tract-binding protein. Genes & Dev. 5, 1224-1236.

Gooding, C., Clark, F., Wollerton, M.C., Grellscheid, S.N., Groom, H., and Smith, C.W. (2006). A class of human exons with predicted distant branch points revealed by analysis of AG dinucleotide exclusion zones. Genome Biol. 7, R1.

Gooding, C., Kemp, P., and Smith, C.W.J. (2003). A novel polypyrimidine tract-binding protein paralog expressed in smooth muscle cells. J. Biol. Chem. 278, 15201-15207.

Gooding, C., Roberts, G.C., and Smith, C.W. (1998). Role of an inhibitory pyrimidine element and polypyrimidine tract binding protein in repression of a regulated alpha-tropomyosin exon. RNA 4, 85-100.

Gromak, N., Rideau, A., Southby, J., Scadden, A.D.J., Gooding, C., Hüttelmaier, S., Singer, R.H., and Smith, C.W.J. (2003). The PTB interacting protein raver1 regulates alpha-tropomyosin alternative splicing. EMBO J. 22, 6356-6364.

Henneberg, B., Swiniarski, S., Becke, S., and Illenberger, S. (2010). A conserved peptide motif in Raver2 mediates its interaction with the polypyrimidine tract-binding protein. Exp. Cell Res. 316, 966-979.

Hüttelmaier, S., Illenberger, S., Grosheva, I., Rüdiger, M., Singer, R.H., and Jockusch, B.M. (2001). Raver1, a dual compartment protein, is a ligand for PTB/hnRNPI and microfilament attachment proteins. J. Cell Biol. 155, 775-786.

Izquierdo, J.M., Majos, N., Bonnal, S., Martinez, C., Castelo, R., Guigo, R., Bilbao, D., and Valcarcel, J. (2005). Regulation of Fas alternative splicing by antagonistic effects of TIA-1 and PTB on exon definition. Mol. Cell 19, 475-484.

Jones, T.A., Zou, J.Y., Cowan, S.W., and Kjeldgaard (1991). Improved methods for building protein models in electron density maps and the location of errors in these models. Acta Crystallogr. A47, 110-119.

Kafasla, P., Morgner, N., Pöyry, T.A.A., Curry, S., Robinson, C.V., and Jackson, R.J. (2009). Polypyrimidine tract binding protein stabilizes the encephalomyocarditis virus IRES structure via binding multiple sites in a unique orientation. Mol. Cell 34, 556-568.

Kielkopf, C.L., Rodionova, N.A., Green, M.R., and Burley, S.K. (2001). A novel peptide recognition mode revealed by the X-ray structure of a core U2AF35/U2AF65 heterodimer. Cell 106, 595-605.

Kleinhenz, B., Fabienke, M., Swiniarski, S., Wittenmayer, N., Kirsch, J., Jockusch, B.M., Arnold, H.H., and Illenberger, S. (2005). Raver2, a new member of the hnRNP family. FEBS Lett. 579, 4254-4258.

Lamichhane, R., Daubner, G.M., Thomas-Crusells, J., Auweter, S.D., Manatschal, C., Austin, K.S., Valniuk, O., Allain, F.H.-T., and Rueda, D. (2010). RNA looping by PTB: Evidence using FRET and NMR spectroscopy for a role in splicing repression. Proc. Natl .Acad. Sci. USA 107, 4105-4110.

Lee, J.H., Rangarajan, E.S., Yogesha, S.D., and Izard, T. (2009). Raver1 interactions with vinculin and RNA suggest a feed-forward pathway in directing mRNA to focal adhesions. Structure 17, 833-842.

Lin, C.H., and Patton, J.G. (1995). Regulation of alternative 3' splice site selection by constitutive splicing factors. RNA 1, 234-245.

Llorian, M., Schwartz, S., Clark, T.A., Hollander, D., Tan, L.-Y., Spellman, R., Gordon, A., Schweitzer, A.C., De La Grange, P., Ast, G., and Smith, C.W.J. (2010). Position-dependent alternative splicing activity revealed by global profiling of alternative splicing events regulated by PTB. Nat. Struct. Mol. Biol. 17, 1114-1123.

Luco, R., Pan, Q., Tominaga, K., Blencowe, B., Pereira-Smith, O., and Misteli, T. (2010). Regulation of alternative splicing by histone modifications. Science 327, 996-1000.

Makeyev, E.V., Zhang, J., Carrasco, M.A., and Maniatis, T. (2007). The MicroRNA miR-124 promotes neuronal differentiation by triggering brain-specific alternative pre-mRNA splicing. Mol. Cell 27, 435-448.

Markovtsov, V., Nikolic, J.M., Goldman, J.A., Turck, C.W., Chou, M.Y., and Black, D.L. (2000). Cooperative assembly of an hnRNP complex induced by a tissue-specific homolog of polypyrimidine tract binding protein. Mol. Cell. Biol. 20, 7463-7479.

Matlin, A.J., Clark, F., and Smith, C.W.J. (2005). Understanding alternative splicing: towards a cellular code. Nat. Rev. Mol. Cell Biol. 6, 386-398.

McCoy, A.J., Grosse-Kunstleve, R.W., Adams, P.D., Winn, M.D., and al., e. (2007). Phaser crystallographic software. J. Appl. Crystallogr. 40, 658-674.

Nilsen, T.W., and Graveley, B.R. (2010). Expansion of the eukaryotic proteome by alternative splicing. Nature 463, 457-463.

Oberstrass, F.C., Auweter, S.D., Erat, M., Hargous, Y., Henning, A., Wenter, P., Reymond, L., Amir-Ahmady, B., Pitsch, S., Black, D.L., and Allain, F.H.-T. (2005). Structure of PTB bound to RNA: specific binding and implications for splicing regulation. Science 309, 2054-2057.

Patton, J.G., Mayer, S.A., Tempst, P., and Nadal-Ginard, B. (1991). Characterization and molecular cloning of polypyrimidine tract-binding protein: a component of a complex necessary for pre-mRNA splicing. Genes Dev. 5, 1237-1251.

Pérez, I., Lin, C.H., McAfee, J.G., and Patton, J.G. (1997). Mutation of PTB binding sites causes misregulation of alternative 3' splice site selection in vivo. RNA 3, 764-778.

Petoukhov, M.V., Monie, T.P., Allain, F.H.-T., Matthews, S., Curry, S., and Svergun, D.I. (2006). Conformation of polypyrimidine tract binding protein in solution. Structure 14, 1021-1027.

Polydorides, A.D., Okano, H.J., Yang, Y.Y., Stefani, G., and Darnell, R.B. (2000). A brain-enriched polypyrimidine tract-binding protein antagonizes the ability of Nova to regulate neuron-specific alternative splicing. Proc. Natl. Acad. Sci. USA 97, 6350-6355.

Ray, D., Kazan, H., Chan, E.T., Peña Castillo, L., Chaudhry, S., Talukder, S., Blencowe, B.J., Morris, Q., and Hughes, T.R. (2009). Rapid and systematic analysis of the RNA recognition specificities of RNA-binding proteins. Nat. Biotechnol. 27, 667-670.

Rideau, A.P., Gooding, C., Simpson, P.J., Monie, T.P., Lorenz, M., Hüttelmaier, S., Singer, R.H., Matthews, S., Curry, S., and Smith, C.W.J. (2006). A peptide motif in Raver1 mediates splicing repression by interaction with the PTB RRM2 domain. Nat. Struct. Mol. Biol. 13, 839-848.

Robinson, F., and Smith, C.W.J. (2006). A splicing repressor domain in polypyrimidine tract-binding protein. J. Biol. Chem. 281, 800-806.

Sawicka, K., Bushell, M., Spriggs, K.A., and Willis, A.E. (2008). Polypyrimidine-tract-binding protein: a multifunctional RNA-binding protein. Biochem. Soc. Trans. 36, 641-647.

Sharma, S., Kohlstaedt, L.A., Damianov, A., Rio, D.C., and Black, D.L. (2008). Polypyrimidine tract binding protein controls the transition from exon definition to an intron defined spliceosome. Nat. Struct. Mol. Biol. 15, 183-191.

Sharma, S., Maris, C., Allain, F.H.-T., and Black, D.L. (2011). U1 snRNA Directly Interacts with Polypyrimidine Tract-Binding Protein during Splicing Repression. Mol. Cell 41, 579-588.

Simpson, P.J., Monie, T.P., Szendröi, A., Davydova, N., Tyzack, J.K., Conte, M.R., Read, C.M., Cary, P.D., Svergun, D.I., Konarev, P.V., et al. (2004). Structure and RNA interactions of the N-terminal RRM domains of PTB. Structure 12, 1631-1643.

Singh, R., Valcárcel, J., and Green, M.R. (1995). Distinct binding specificities and functions of higher eukaryotic polypyrimidine tract-binding proteins. Science 268, 1173-1176.

Tillmar, L., Carlsson, C., and Welsh, N. (2002). Control of insulin mRNA stability in rat pancreatic islets. Regulatory role of a 3'-untranslated region pyrimidine-rich sequence. J. Biol. Chem. 277, 1099-1106.

Tunnicliffe, R.B., Hautbergue, G.M., Kalra, P., Jackson, B.R., Whitehouse, A., Wilson, S.A., and Golovanov, A.P. (2011). Structural basis for the recognition of cellular mRNA export factor REF by herpes viral proteins HSV-1 ICP27 and HVS ORF57. PLoS Path. 7, e1001244.

Wagner, E.J., and Garcia-Blanco, M.A. (2001). Polypyrimidine tract binding protein antagonizes exon definition. Mol. Cell. Biol. 21, 3281-3288.

Witten, J.T., and Ule, J. (2011). Understanding splicing regulation through RNA splicing maps. Trends Genet. 27, 89-97.

Xue, Y., Zhou, Y., Wu, T., Zhu, T., Ji, X., Kwon, Y.-S., Zhang, C., Yeo, G., Black, D.L., Sun, H., et al. (2009). Genome-wide analysis of PTB-RNA interactions reveals a strategy used by the general splicing repressor to modulate exon inclusion or skipping. Mol. Cell 36, 996-1006.

Yamamoto, H., Tsukahara, K., Kanaoka, Y., Jinno, S., and Okayama, H. (1999). Isolation of a mammalian homologue of a fission yeast differentiation regulator. Mol. Cell. Biol. 19, 3829-3841.

Zou, P., Gautel, M., Geerlof, A., Wilmanns, M., Koch, M.H., and Svergun, D.I. (2003). Solution scattering suggests cross-linking function of telethonin in the complex with titin. J. Biol. Chem. 278, 2636-2644.

Link to original article:

http://www.cell.com/structure/abstract/S0969-2126(11)00333-9

Figure S1 (related to Fig. 1): Crystallographic results for Raver1 PRIs bound to PTB RRM2.

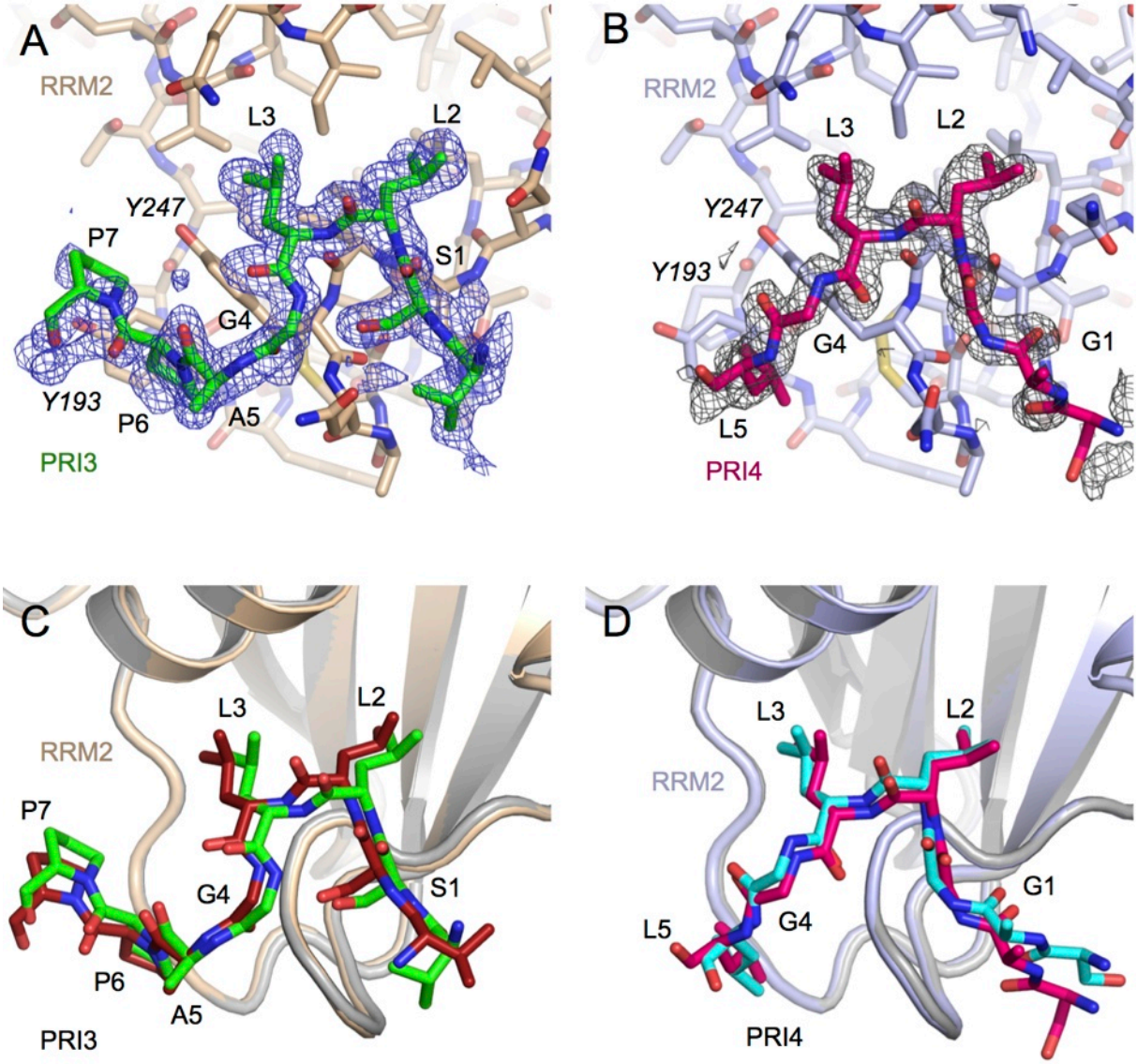

Simulated annealing F_o-F_c omit maps of (A) PRI3-RRM2 and (B) PRI4-RRM2, both phased in the absence of a model for the PRI peptide. (C) Comparison of molecules A and B from the crystal asymmetric unit of PRI3. (D) Comparison of molecules A and B from the crystal asymmetric unit of PRIs 3 and 4 respectively.

Figure S2: Comparison of the X-ray structure with NOEs measured in solution.

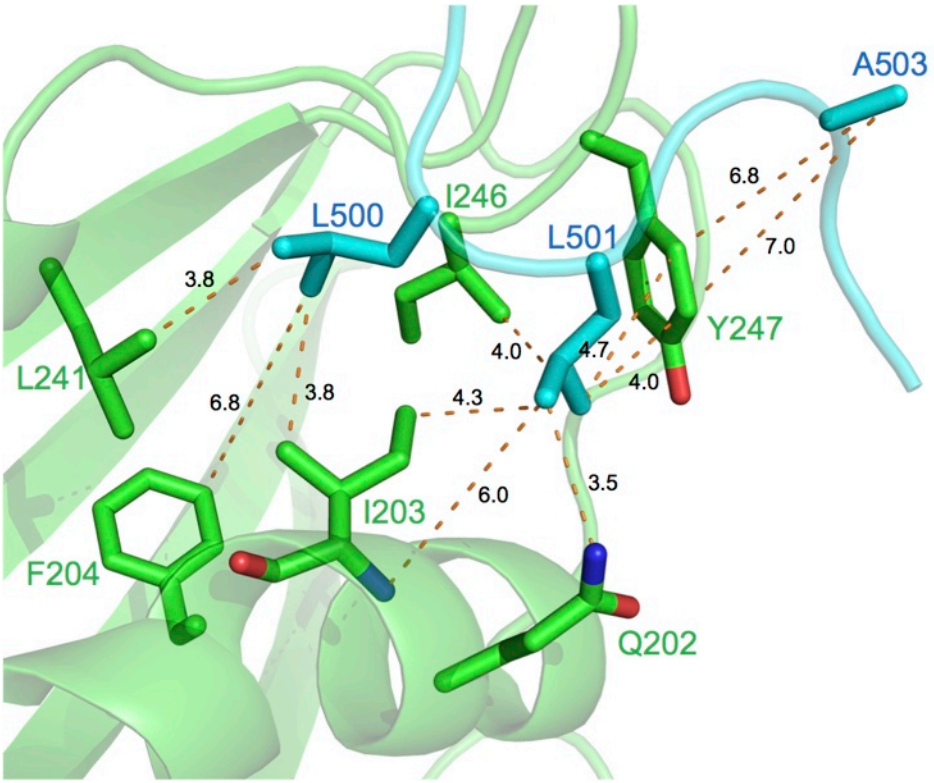

The 11 NOEs observed in the previous NMR study of the RRM2 complex with Raver1 peptide (Rideau et al., 2006) are shown as dashed lines on the X-ray structure determined here. RRM2 is coloured green, Raver1 cyan, with key side-chains drawn as sticks. The distances shown are carbon-carbon or carbon-nitrogen and are taken from the crystal structure. As the NOEs are between hydrogen atoms, in most cases the distances shown greatly overestimate the actual distance measured by NMR. The structure is thus consistent with the NMR data, with the exception of the position of Ala 503 on Raver1, which on average is closer in the dynamic solution ensemble detected by NMR that was observed in the crystal structure. This discrepancy may be due to increased mobility of the bound peptide in the solution structure, as compared to the crystallised complex.

Figure S3 (Related to Fig. 3): PTB and PTB homologues have the same affinity for PRIs.

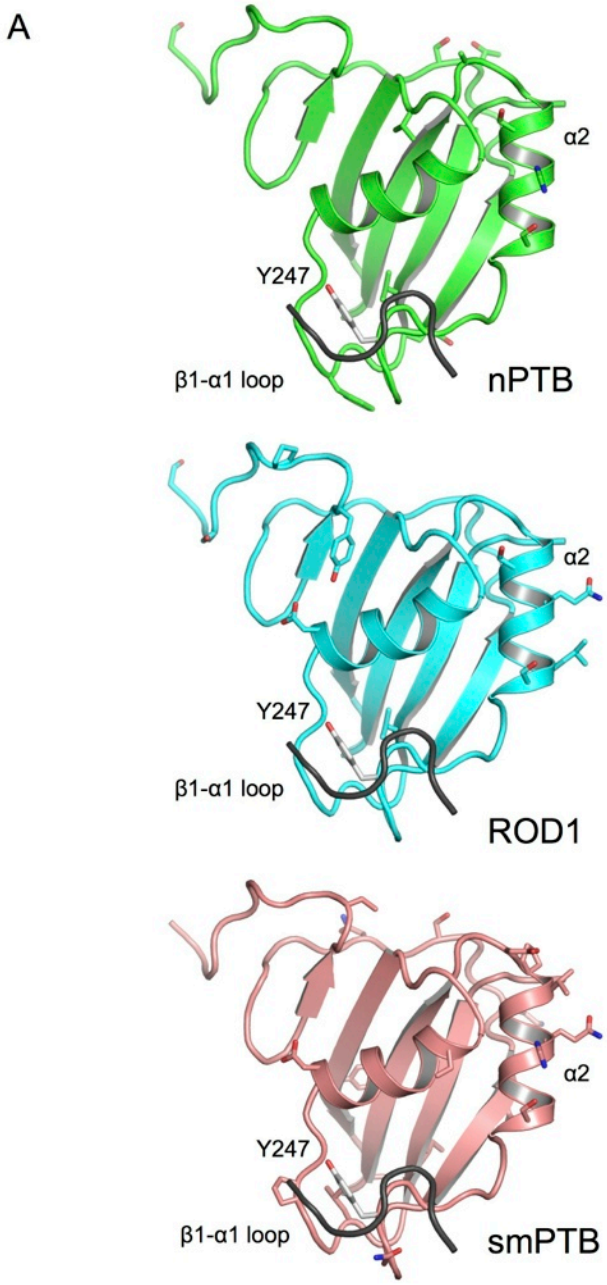

(A) Mapping of sequence differences between PTB and nPTB, ROD1 and smPTB onto the structure of the Raver1-PTB complex (PRI3-RRM2). Residues from PTB that are altered in the three paralogues are shown as sticks. Y247, which is conserved between the paralogues, is also shown.

Figure S3 (Related to Fig. 3; cont.): PTB and PTB homologues have the same affinity for PRIs. (cont.)

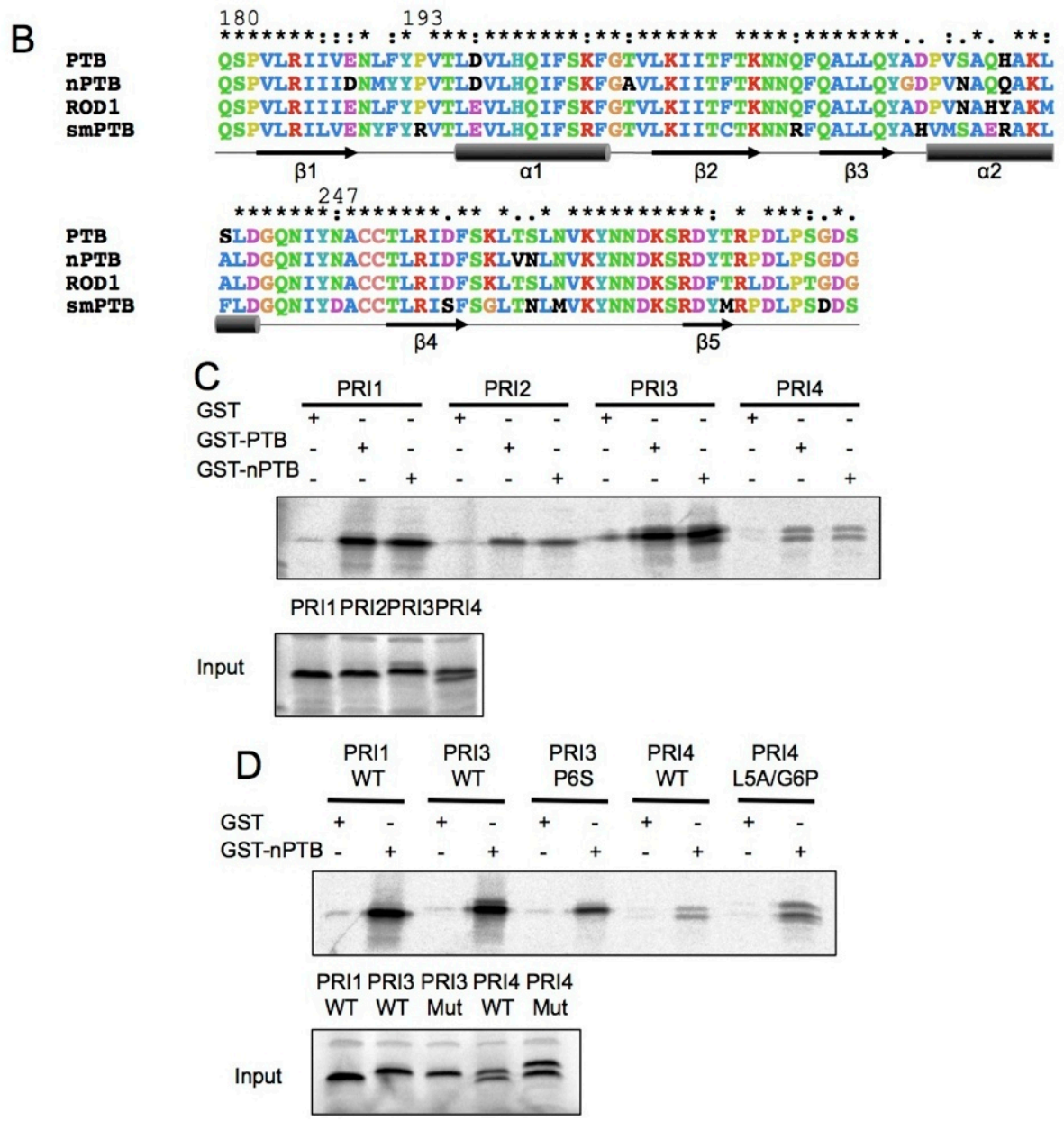

(B) Alignment of RRM2 sequences for PTB paralogues. (C) GST-pulldown of Raver1 PRIs with 2 μg GST or 6 μg GST-PTB or GST-nPTB. (D) GST pulldown of Raver1 PRIs 1, 3 and 4 and mutants (PRI3 P6S and PRI4 L5A/G6P) with 2 μg GST or 6 μg GST-nPTB.

Figure S4 (Related to Fig. 5): Superposition of the structure of the PRI3-RRM2 complex with the ICP27/ REF peptide-RRM complex.

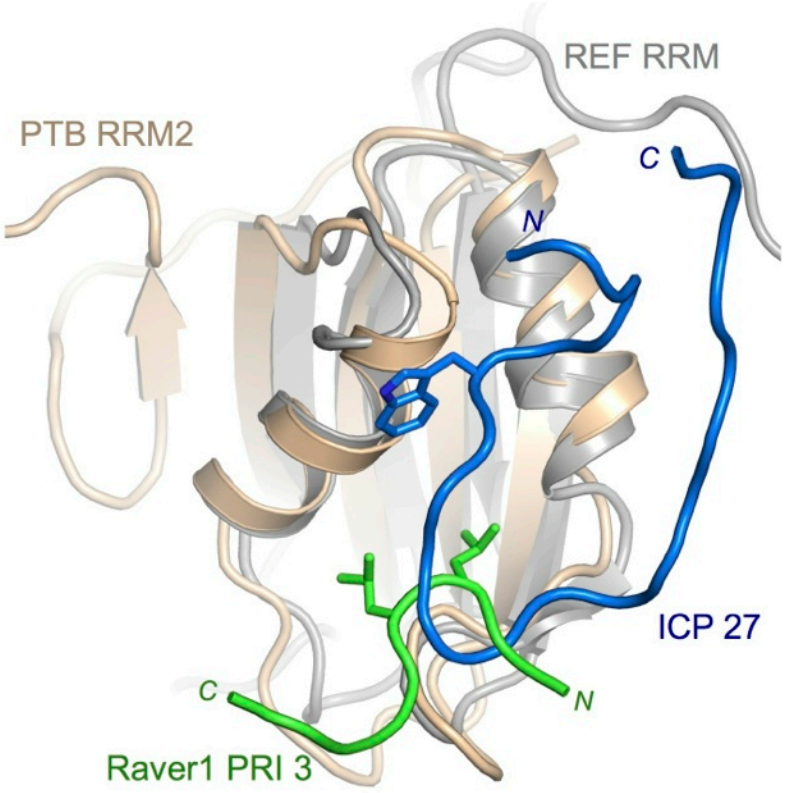

The Raver1 peptides (green) bind perpendicular to the helices of PTB RRM2 (tan) inserting two leucines (shown as sticks) into a shallow hydrophobic pocket. In contrast, the peptide from ICP27 (blue) binds in an orientation that is *parallel* to dorsal helices in the REF2 RRM (grey) (Tunnicliffe et al., 2011). The ICP27/REF complex nevertheless displays some similarity with other peptide/RRM complexes since the ICP27 peptide inserts a tryptophan side chain into a hydrophobic pocket between the helices to stabilise the interaction.

REFERENCES

Rideau, A.P., Gooding, C., Simpson, P.J., Monie, T.P., Lorenz, M., Hüttelmaier, S., Singer, R.H., Matthews, S., Curry, S., and Smith, C.W.J. (2006). A peptide motif in Raver1 mediates splicing repression by interaction with the PTB RRM2 domain. Nat. Struct. Mol. Biol. *13*, 839-848.

Tunnicliffe, R.B., Hautbergue, G.M., Kalra, P., Jackson, B.R., Whitehouse, A., Wilson, S.A., and Golovanov, A.P. (2011). Structural basis for the recognition of cellular mRNA export factor REF by herpes viral proteins HSV-1 ICP27 and HVS ORF57. PLoS Path. *7*, e1001244.

Original article can be found at: http://www.cell.com/structure/abstract/S0969-2126(11)00333-9